

# Infraslow Electroencephalographic and Dynamic Resting State Network Activity

Joshua K. Grooms,<sup>1,\*</sup> Garth J. Thompson,<sup>2,\*</sup> Wen-Ju Pan,<sup>1</sup> Jacob Billings,<sup>3</sup>  
Eric H. Schumacher,<sup>4</sup> Charles M. Epstein,<sup>5</sup> and Shella D. Keilholz<sup>1,3</sup>

## Abstract

A number of studies have linked the blood oxygenation level dependent (BOLD) signal to electroencephalographic (EEG) signals in traditional frequency bands ( $\delta$ ,  $\theta$ ,  $\alpha$ ,  $\beta$ , and  $\gamma$ ), but the relationship between BOLD and its direct frequency correlates in the infraslow band ( $<1$  Hz) has been little studied. Previously, work in rodents showed that infraslow local field potentials play a role in functional connectivity, particularly in the dynamic organization of large-scale networks. To examine the relationship between infraslow activity and network dynamics in humans, direct current (DC) EEG and resting state magnetic resonance imaging data were acquired simultaneously. The DC EEG signals were correlated with the BOLD signal in patterns that resembled resting state networks. Subsequent dynamic analysis showed that the correlation between DC EEG and the BOLD signal varied substantially over time, even within individual subjects. The variation in DC EEG appears to reflect the time-varying contribution of different resting state networks. Furthermore, some of the patterns of DC EEG and BOLD correlation are consistent with previous work demonstrating quasiperiodic spatiotemporal patterns of large-scale network activity in resting state. These findings demonstrate that infraslow electrical activity is linked to BOLD fluctuations in humans and that it may provide a basis for large-scale organization comparable to that observed in animal studies.

**Keywords:** DC-EEG; functional connectivity; infraslow; resting state MRI; sliding window correlation

## Introduction

**R**ESTING STATE FUNCTIONAL magnetic resonance imaging (rs-fMRI) is at the forefront of research on the brain's large-scale organization. However, the slow spontaneous fluctuations of the blood oxygenation level dependent (BOLD) signal used to map functional connectivity at rest have been less studied than their task-related cousins. A number of previous studies in rodents and humans have probed the relationship between electrical activity in typical electroencephalographic (EEG) bands and the BOLD signal, and while it is clear that the spontaneous BOLD fluctuations reflect changes in neural activity, the relationship between the two is not well understood. Several studies using invasive microelectrode recording in animals point to gamma band activity as being most closely related to the local BOLD fluctuations

(Logothetis et al., 2001; Pan et al., 2011; Shmuel and Leopold, 2008), but coordinated delta and theta activity have been linked to interhemispheric BOLD correlations (Lu et al., 2007; Pan et al., 2011). Recent work by Pan et al. (2013) has also shown the infraslow electrical analogues of the BOLD frequencies, which are relatively little studied in traditional experiments, and are in fact strong contributors to the local BOLD fluctuations and interhemispheric correlation. (While the terminology for electrical frequencies below 1 Hz is not standardized, for this and previous studies we designate activity in the same approximate frequency range as the BOLD fluctuations [0.01 to 0.1 Hz] as the infraslow EEG band.) A deeper examination of the relationship between the infraslow activity and the BOLD signal demonstrated that infraslow activity contributes to quasiperiodic patterns (QPPs) of spatial and temporal changes in the

<sup>1</sup>Department of Biomedical Engineering, Georgia Institute of Technology and Emory University, Atlanta, Georgia.

<sup>2</sup>Magnetic Resonance Research Center (MRRC) and Radiology and Biomedical Imaging, Yale University, New Haven, Connecticut.

<sup>3</sup>Department of Neuroscience, Emory University, Atlanta, Georgia.

<sup>4</sup>Department of Psychology, Georgia Institute of Technology, Atlanta, Georgia.

<sup>5</sup>Department of Neurology, Emory University School of Medicine, Atlanta, Georgia.

\*These authors contributed equally to this work.

BOLD signal that have been observed in rats and humans (Majeed et al., 2009, 2011; Thompson et al., 2014b), indicating that it may also play a role in network dynamics.

Similar attempts to understand the neural basis of rs-fMRI in healthy humans are limited to noninvasive measures from outside the brain using EEG or magnetoencephalography (MEG). These methods measure less localized activity compared to the invasive recordings in animals, and sensitivity is primarily limited to the brain's surface. Despite these challenges, a recent article by Hiltunen et al. (2014) provided the first direct evidence of coupling between independent components (ICs) of the full-band EEG signal (0–250 Hz) and resting state BOLD networks. The voxel-wise correlation between certain components and the BOLD signal strongly resembled resting state networks, including the default mode network (DMN). This is promising evidence that the relationship between infraslow activity and the BOLD signal observed in rats is also present in humans. However, the Hiltunen et al. article did not examine the relationship between directly measured infraslow activity and BOLD, instead using ICs of the full-band EEG signal that were then downsampled and convolved with a gamma function before correlation with the BOLD signal, making the role of infraslow activity in the BOLD network correlations difficult to interpret.

This study builds upon the work by Hiltunen et al. by demonstrating a direct link between the BOLD signal and infraslow EEG as measured in electrode space. Moreover, we examine the role that infraslow activity plays in two types of network dynamics. The quasiperiodic spatiotemporal patterns of BOLD activity observed in rats can also be detected in humans and are particularly interesting due to the alternation between the DMN and the task positive network (TPN) that occurs in the patterns (Majeed et al., 2011). In rats, these QPPs are linked to infraslow electrical activity. We examine the patterns of BOLD and infraslow correlation for evidence of a similar link in humans. The second type of network dynamic involves interactions within and between brain networks (Chang and Glover, 2010; Grigg and Grady, 2010; Handwerker et al., 2012; Hutchison et al., 2013; Keilholz, 2014; Keilholz et al., 2013; Leonardi and Van De Ville, 2015; Liu and Duyn, 2013; Majeed et al., 2009, 2011). We utilize sliding window correlation to determine whether the relationship between infraslow EEG and BOLD varies over time. Our results shed light on the neural processes that underlie the network dynamics measured with BOLD MRI.

## Materials and Methods

### *Experimental protocol*

All studies were approved by the Georgia Institute of Technology Institutional Review Board. Written informed consent was obtained from 10 healthy subjects (4 female/6 male; 18–39 years). Data acquisition was performed on the 3T Siemens scanner at the joint Georgia State University/Georgia Institute of Technology Center for Advanced Brain Imaging.

Subjects participated in a single session that included an anatomical scan and four individual functional scans lasting ~10 min each. For every functional scan, EEG and fMRI were simultaneously recorded. Of the four scans that were acquired per session, the first two were recorded while in the resting state, with subjects lying motionless in the scan-

ner with eyes fixated on a small dot at the center of the visual field. Subjects were instructed to remain awake but to otherwise let their minds wander freely. In contrast, the task state that took place during the latter two scans consisted of subjects performing a psychomotor vigilance task (Dinges and Powell, 1985; Thompson et al., 2013). This task involved monitoring a dot for randomly occurring color changes and pushing a button immediately after the change was perceived. The data recorded during the task were not utilized for the current study, but is included in the description of the procedure for the sake of completeness.

**Electroencephalography.** Electrodes were positioned according to the standard International 10-10 System montage and were permanently affixed to a cap that incorporated electrodes fabricated with reusable sintered Ag/AgCl and safety resistors, supplied as part of the Neuroscan system (Neuroscan Systems, Charlotte, NC). Subjects washed their scalps within 12 h of recording. Further skin preparation included initial abrasion by a stiff hair brush, gentle rubbing with a commercial abrasive prep, and alcohol wipe. Impedances below 5000 ohms were verified by direct measurement. Before the start of a scanning session, the cap itself was aligned on the scalp using common skull landmarks. The skin was slightly abraded beneath each contact to improve the connection. Redux electrolyte crème (Parker, Fairfield, NJ) was used. Continuous direct current (DC) EEG was simultaneously recorded from 68 sintered Ag/AgCl electrodes for each participant. Electrode data were transmitted to a DC-capable SynAmps2 amplifier (Neuroscan Systems, Charlotte, NC) located outside of the scanner room. Signals were digitized at a passband of 0–300 Hz, a 24 bit amplitude resolution, and a sampling frequency of 10 kHz.

**Magnetic resonance imaging.** Imaging was performed on a Siemens Trio 3T whole body MRI scanner. A three-plane localizer was first used to determine positioning. Structural images with 1 mm isotropic voxels were then acquired for each participant using a T1-weighted MP RAGE 3D sequence (FOV 220 × 220 mm<sup>2</sup>; matrix size 256 × 256; 176 1 mm slices; TR 2250 msec; TE 4 msec; TI 850 msec; flip angle 9°). Functional data were recorded for two consecutive resting state scans using an echo-planar imaging (EPI) sequence with an echo time (TE) of 30 msec; a repetition time (TR) of 2 sec; matrix size 64 × 64; 33 axial slices covering the whole brain; spatial resolution of ~3.4 mm isotropic; and 476 repetitions.

### *Preprocessing*

fMRI data preprocessing followed typical procedures for functional connectivity studies (Faro and Mohamed, 2010; Poldrack et al., 2011). The following preprocessing steps were done in Statistical Parametric Mapping 8 (SPM8; Wellcome Department of Cognitive Neurology, London, United Kingdom) using the MarsBaR region of interest plug-in: T1 images were segmented into gray matter, white matter, and cerebrospinal fluid maps. These were used to generate corresponding masks that could be applied to the BOLD volumes. EPI data were first slice-time corrected and then motion corrected through registration to a mean of all EPI images using Analysis of Functional NeuroImages (AFNI; Cox, 1996). From AFNI the maximum total movement in

each direction (X, Y, and Z) was recorded. Motion parameters were regressed out. Next, images were registered to their anatomical counterparts and normalized to MNI spatial coordinates to facilitate comparisons between individuals.

From this point forward, custom-written MATLAB routines were used for analysis. BOLD data sets were spatially blurred using a 3D Gaussian kernel [sized  $3 \times 3 \times 1$  voxels,  $\sigma = (2, 2, 1)$  voxels]. The time series of each voxel was then FIR filtered to a passband of 0.01–0.08 Hz (slightly less than the full infraslow range of 0.01–0.1 Hz to follow conventional processing procedures for resting state MRI data). Following this step, the first 22 volumes of each scanning trial were discarded to account for both MR stabilization effects and the phase delay that filtering imposed. Quadratic detrending was performed to remove drift artifacts. As shown in Thompson et al. (2016), the frequencies affected by detrending form a negative exponential with the greatest effect under 0.005 Hz and little effect in the range from 0.01 to 0.08 Hz. The effects of quadratic and linear detrends on the frequency profile are nearly identical. Each voxel was z-scored over time. This reexpresses voxel signal amplitude as a fraction of its standard deviation and centers it about zero.

EEG data were preprocessed through the MATLAB toolbox EEGLAB (Delorme and Makeig, 2004). MRI gradient switching artifacts were first removed using the Bergen EEG-fMRI Toolbox (Moosmann et al., 2009). EEG signals were then synchronized with the functional imaging data using the known temporal locations of MRI gradient switching artifacts. Ballistocardiographic artifacts were removed next with the FMRIB plug-in for EEGLAB. This tool operates by subtracting a template from each channel time series that is constructed based on QRS events (Niazy et al., 2005). EEG signals were then FIR filtered to a final passband of 0.01–0.08 Hz and downsampled to match the BOLD sampling rate. As with the functional data, the first 22 samples were discarded to account for phase delay and maintain synchronicity with BOLD signals. Quadratic detrending was also performed to eliminate drift artifacts. Finally, each EEG signal was z-scored across time.

#### Data exclusion

Head motion did not exceed the width of a voxel on any trial so no data were removed for excessive motion. However, a total of four participants (eight trials) were excluded for different reasons. For one participant, corrupted EEG data files were discovered after the scanning session. A second participant was excluded upon finding that an irregular electrode ordering scheme had been used while recording EEG data. In this case, the true scalp electrodes from which the recorded signals originated could not be determined with certainty. Two additional participants (four trials) were excluded due to the presence of large artifacts in the EEG data that could neither be explained nor adequately removed. These artifacts were found across all electrodes and effectively obscured any neurophysiological data that might have been acquired.

#### Examination for volume conduction

Volume conduction is a well-known phenomenon in electrophysiology that is characterized by a near-instantaneous spread

of current from a single source (Stam et al., 2007) that may or may not be remotely relative to the electrode site (Khader et al., 2008). Because volume conduction is practically instantaneous, it should manifest as large clusters of electrodes that are most similar to one another without any time delay. To check for this effect, EEG data from each electrode were cross-correlated pairwise at a range of time offsets to determine the time at which maximum correlation was achieved.

#### Choice of electrodes

A comparison between all 68 channels of EEG data and all voxels of a functional image volume would require extensive correction for the large number of multiple comparisons and would impose heavy computational demands. By choosing regionally representative electrodes across the scalp, much of the available spatial information can be preserved while ameliorating the multiple comparisons and colinearity problems. The electrodes that were chosen for detailed examination were as follows: FPz, FT7, FCz, FT8, TP9, CPz, TP10, PO9, POz, and PO10 (see the blue highlighted electrodes in Fig. 1 for the spatial layout of this subset). This set of 10 electrodes provided evenly distributed brain coverage in the anterior-to-posterior and left-to-right directions. In addition, these particular electrodes contained data that were free of any obvious artifacts across all scans that were used.

#### Steady-state analysis

For each individual scan, the time courses from each of the 10 selected EEG channels were cross-correlated with the BOLD time course from every voxel to produce spatial mappings of the linear relationship between them as a function of temporal offset.

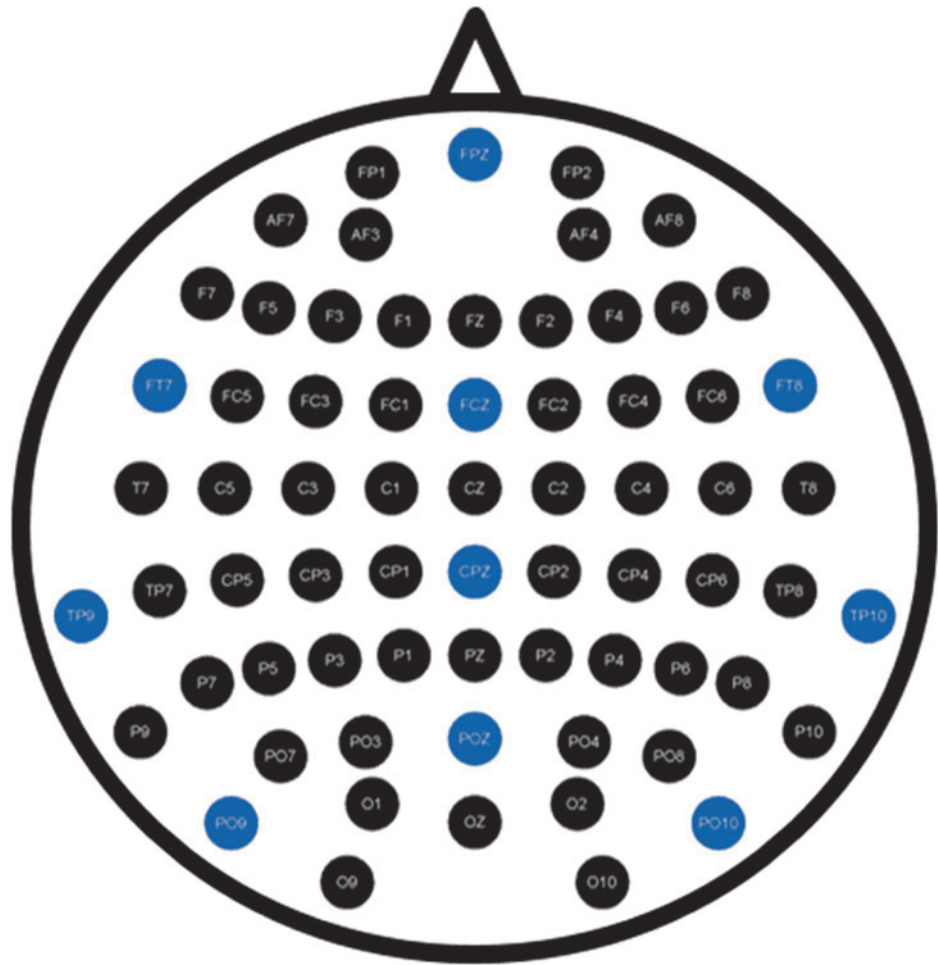
$$r_{n(x,y)} = \frac{\sum_{i=1}^T (v(x,y)_i - \bar{v}(x,y))(elc_{n,i} - \overline{elc_n})}{\sqrt{\sum_{i=1}^T (v(x,y)_i - \bar{v}(x,y))^2} \sqrt{\sum_{i=1}^T (elc_{n,i} - \overline{elc_n})^2}}$$

where  $r_{n(x,y)}$  is the correlation between the time course of electrode  $n$  ( $elc_n$ ) and the time course of voxel  $v(x, y)$ , and  $T$  is the number of time points in the scan. A bar over the variable indicates the mean over the time course. This calculation was repeated for each time lag.

A total of 21 offsets, ranging between [–20 sec, 20 sec] in steps of one TR (2 sec), were tested between the signals. This range is wide enough to capture a complete quasiperiodic spatiotemporal pattern as described in Majeed et al. (2011) and can be examined for evidence of a link between the QPP and infraslow activity as in Thompson et al. (2014b) and Pan et al. (2013). Every resulting correlation coefficient was then converted to a standard z-score using the corrected Fisher Transform for filtered time series. Finally, coefficients were averaged across all scans in a fixed effects analysis and tested for statistical significance.

To identify BOLD resting state networks (RSNs) for further analysis, spatial ICA was performed using the GIFT toolbox for MATLAB (<http://mialab.mrn.org/software>). The number of output components was heuristically estimated at 20, and the Infomax algorithm (Bell and Sejnowski, 1995) was used as the objective function to maximize independence. The resulting ICs were identified by visually comparing them to the literature. The majority of the ICs

**FIG. 1.** Ten EEG channels (highlighted in blue) forming a subset of the complete montage that were chosen for direct comparisons with BOLD data. Subset channels evenly covered the scalp and contained valid electrophysiological data in every trial. All EEG mappings throughout this document are oriented identically to this figure. Starting from the top (nasion direction) and moving left-to-right toward the bottom (inion direction), the highlighted channels are: FPz, FT7, FCz, FT8, TP9, CPz, TP10, PO9, POz, and PO10. BOLD, blood oxygenation level dependent; EEG, electroencephalography. Color images available online at [www.liebertpub.com/brain](http://www.liebertpub.com/brain)



were easily recognizable and correspond well with known RSN topographies (Damoiseaux et al., 2006; Lee et al., 2013; Rosazza and Minati, 2011; Veer et al., 2010) or brain structures. During the course of decomposition, GIFT automatically back-reconstructs and saves a time series for each resolved IC per individual trial, which are representative of the regional average BOLD signals (Calhoun et al., 2001). The time course from each RSN was then correlated with the time course from every EEG electrode to determine the extent to which each RSN was driving the signal at each electrode.

$$r_{n,j} = \frac{\sum_{i=1}^T (rsn_{n,i} - \overline{rsn_n})(elc_{j,i} - \overline{elc_j})}{\sqrt{\sum_{i=1}^T (rsn_{n,i} - \overline{rsn_n})^2} \sqrt{\sum_{i=1}^T (elc_{j,i} - \overline{elc_j})^2}}$$

where  $r_{n,j}$  is the correlation between the time course of electrode  $j$  ( $elc_j$ ) and the time course of the RSN  $n$  ( $rsn_n$ ), and  $T$  is the number of time points in the scan. A bar over the variable indicates the mean over the time course.

#### Dynamic analysis

To determine if the relationship between EEG and BOLD varied over time, SWC time series between all BOLD voxels of a trial and each of the 10 members of the EEG electrode subset was computed. Window length

was fixed at 50 sec (50 sec =  $1/(2 \times 0.01)$  Hz), as suggested in Sakoğlu et al. (2010) and Thompson et al. (2013) for both BOLD and EEG data). For this analysis it was necessary to choose a single value for the hemodynamic delay between the BOLD and EEG signals, so BOLD windows were offset 4 sec in the future relative to EEG windows (Miezin et al., 2000). Successive windows along each time series were shifted by one TR. This process is illustrated in Figure 2. Correlation coefficients at each time point were again converted to z-scores. The mean and the standard deviation for histograms of real data and permuted data were calculated.

To determine whether the sliding window correlation between BOLD and EEG reflected combinations of RSNs, the SWC series were decomposed using group sICA and the resulting components were examined for resemblance to RSNs, using the same approach described in Steady-State Analysis section.

#### Quasiperiodic patterns

To perform preliminary examination of the relationship between DC EEG and QPPs of BOLD signal propagation in humans, templates of the QPP were made on a group-wise basis using the algorithm described in Majeed et al. (2011) (template length 40 sec, threshold 0.01 first 10 iterations, and then 0.02 for up to 50 iterations). Briefly, all rs-MRI scans

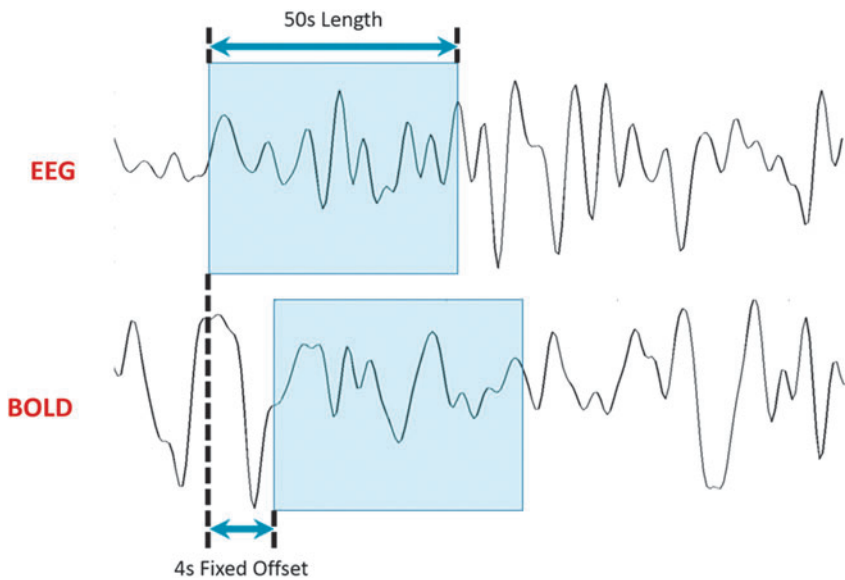


**FIG. 2.** An illustration of the SWC analysis using example infraslow BOLD and EEG data. Successive windows “slide” along each time series (maintaining the offset present), constructing a correlation signal at each increment. SWC, sliding window correlation. Color images available online at [www.liebertpub.com/brain](http://www.liebertpub.com/brain)

from all subjects were concatenated, and a pattern-finding algorithm was applied. The pattern-finding algorithm takes a randomly-selected 4D chunk of data (the template) and calculates correlation in a sliding manner between the template and the entire time course. Instances in the time course with correlation to the template above the threshold are averaged together to make a new template. The process is then repeated until the template converges. A summary of the algorithm is shown in Figure 3. The results were a spatiotemporal template of the QPP and a plot of the strength of the pattern over time across all concatenated subjects. Pearson correlation between the plot of the template strength as a function of time and the DC EEG signal from all electrodes was calculated at 40 time shifts in 2 sec increments, from -40 to 40 sec.

$$r_j = \frac{\sum_{i=1}^T (qpp_i - \overline{qpp})(elc_{j,i} - \overline{elc_j})}{\sqrt{\sum_{i=1}^T (rqqp_i - \overline{qqp})^2} \sqrt{\sum_{i=1}^T (elc_{j,i} - \overline{elc_j})^2}}$$

where  $r_j$  is the correlation between the QPP template strength time course ( $qpp$ ) and the time course of each electrode  $j$  ( $elc_j$ ), and  $T$  is the number of time points in the scan. A bar over the variable indicates the mean over the time course. This calculation was repeated for each time lag.

Correlation between one hundred randomly permuted (without duplication) rs-MRI and EEG pairs was calculated to provide a “null” distribution for comparison. Pearson’s  $r$  values were transformed to  $Z$  as per Equation 3.5 with  $\kappa = N - 3$  ( $N$  being the number of time points correlated;  $N$  varied based on the time shift) (Thompson et al., 2013). Family wise error rate (FWER) control as described below was run across all electrodes and time shifts.

*Statistical significance testing*

Before further analysis, correlation coefficients were Fisher transformed to better approximate a normal distribution (Fisher, 1915). The Fisher Transform is derived under the assumption that the signal time points used to calculate correlation coefficients are bivariate normal. Certain prepro-

cessing steps that are commonly performed on neurophysiological signals, such as blurring and filtering, can easily violate this assumption and, thereby, render typical significance tests invalid (Aguirre et al., 1997; Davey et al., 2013; Lenoski et al., 2008; Worsley and Friston, 1995). In

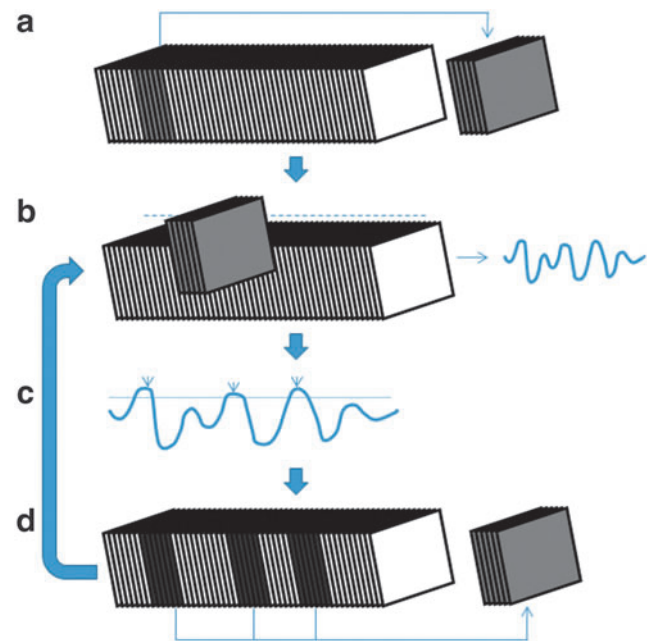


**FIG. 3.** QPP generation. (a) As described in Majeed et al. (2011), the algorithm randomly selects a 4D chunk of data with a specified length (window length). This chunk is designated the template and is correlated with the entire time course in a sliding manner (b). At time points that are similar to the template, correlation values are greater than the threshold (c). These time points are averaged together (d) and the process is repeated (a) until the template converges. The results of the algorithm are the spatiotemporal template and a plot of the correlation between the image time series and the template as a function of time. QPP, quasiperiodic pattern. Color images available online at [www.liebertpub.com/brain](http://www.liebertpub.com/brain)

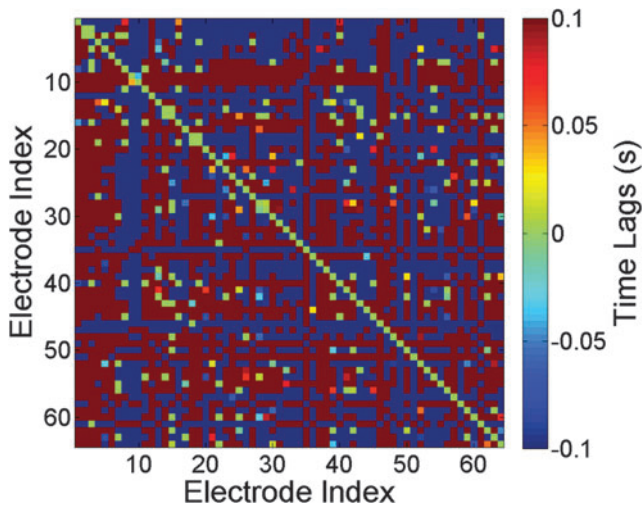


**FIG. 4.** Time delays of maximum correlation between EEG signals as a test for volume conduction from a single representative trial. Colors span an offset range of 200 msec, and most channel pairings require delays well outside of this range to achieve maximum correlation, as can be seen clearly in the figures that follow. Few channels correlate most strongly near 0 sec, a lag which would suggest the presence of volume conduction. Color images available online at [www.liebertpub.com/brain](http://www.liebertpub.com/brain)

such cases, null z-scored correlation values belong not to a standard normal distribution but to a narrower Gaussian distribution that relies on the degrees of freedom ( $\nu$ ) of the data used to generate them:  $z \sim N(0, \nu^{-1})$ . A simple estimator for the effective degrees of freedom of FIR filtered signals was recently derived in Davey et al. (2013) and is calculated using the following equation:

$$\kappa = 2T_s(f_h - f_l)T, \quad (3.4)$$

where  $\kappa$  is the *effective* degrees of freedom,  $T_s$  is the sampling period,  $f_h$  and  $f_l$  are, respectively, the high- and low-pass cutoff frequencies for the FIR filter, and  $T$  is the number of samples in the signal. The corrected Fisher's Transform is then:

$$z = \frac{\arctan(r)}{1/\sqrt{\kappa}} = \sqrt{\kappa} \cdot \operatorname{arctanh}(r). \quad (3.5)$$

Statistical significance of results was assessed using permutation tests (Poldrack et al., 2011). This is a nonparametric approach that estimates confidence intervals for hypothesis tests by empirically constructing a null distribution with shuffled data against which real data sets can be compared. Permuta-

tion tests for this study were performed using all possible inappropriate pairings of trial data, amounting to  $66 = \binom{12}{2}$  sets of data per null distribution. This was expected to break any existing temporal synchronization between neural events in the BOLD and EEG data sets.

Control of FWER for the large numbers of comparisons being made per analysis was accomplished using sequential goodness of fit (Carvajal-Rodriguez et al., 2009). For this study, FWER was fixed at 0.05.

## Results

### Volume conduction

Volume conduction is expected to manifest as instantaneous correlation across channels. A few channel pairings were most strongly correlated at  $\sim 0$  sec offset, but the vast majority required delays in excess of 100 msec to achieve maximum correlation (shown in Fig. 4 for one typical trial). Similar findings across all trials led us to conclude that volume conduction was not a major contributor in this study.

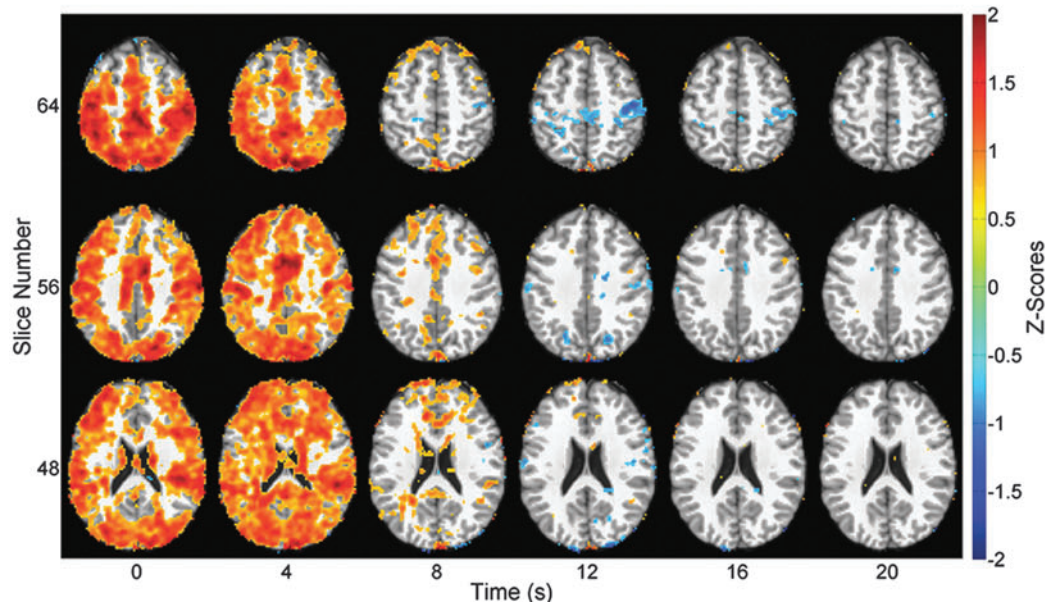
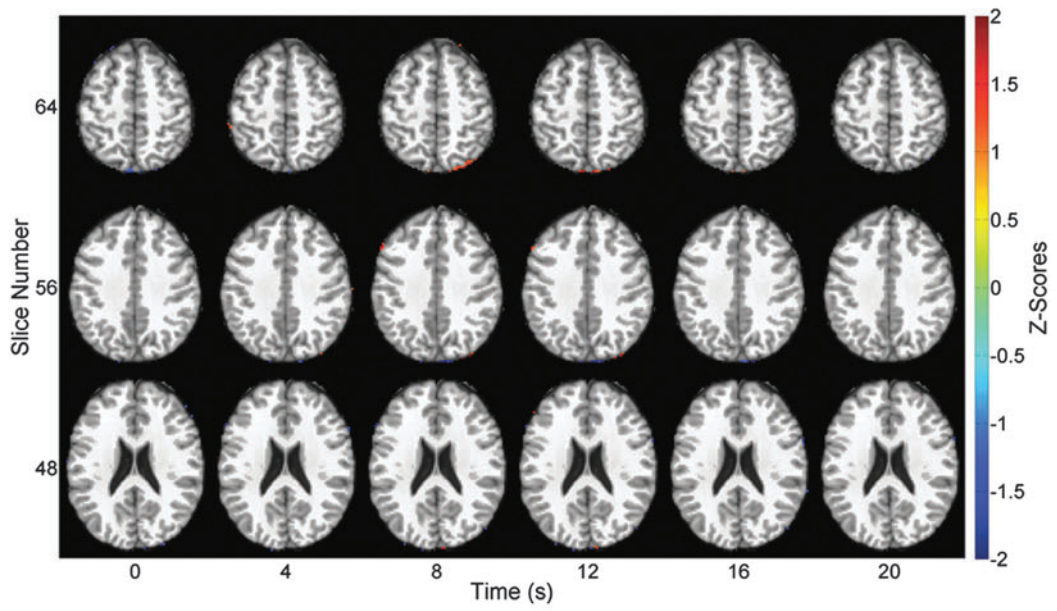
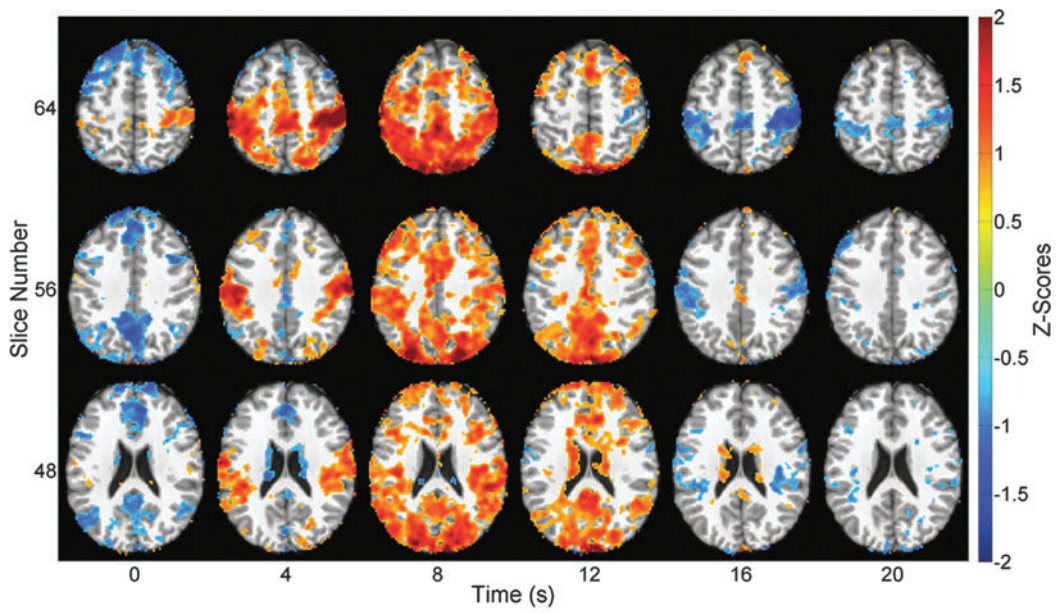
### Stationary analysis

Static correlation of the BOLD signal and the EEG signal from each electrode produced a series of 10 spatiotemporal correlation maps. Representative samples are shown in Figure 5 (remaining data shown in Supplementary Fig. S1; Supplementary Data are available online at [www.liebertpub.com/brain](http://www.liebertpub.com/brain)). Each is a group-wide average of the correlation between a single EEG electrode signal and all BOLD voxel time series at various time shifts.

Although only three representative mappings are shown in this study, the other averages shown in Supplementary Figure S1 exhibit patterns resembling one of them. In general, when correlation is present to any large extent, it almost universally includes both the sensorimotor cortices and intraparietal sulci (IPS). The latter structures are well-known members of the TPN (Fox et al., 2005; Fransson, 2005). In one typical pattern (Fig. 5, top), positive correlation in these regions starts as early as the 0 sec offset, reaches maximal strength at  $\sim 8$  sec, and then vanishes by about 12 sec. Negative correlation in these same regions was then observed to follow a similar trend between  $\sim 12$  and 20 sec. BOLD correlates of FPz, FCz, FT8, CPz, and TP9 all followed this progression of events.

Mappings for the TP10, PO10, and POz electrodes exhibit positive correlations starting at approximately  $-4$  sec, peaking at 0 sec, and nearly vanishing by 8 sec (Fig. 5, bottom). Like

**FIG. 5.** (Top) Group-averaged correlation between infraslow BOLD and the FPz electrode shown for three slices at time lags from 0 to 20 sec. Colored results are significant at FWER of 0.05. Time shifts in seconds refer to the delay imposed on the BOLD relative to EEG signals while calculating correlation. At 0 sec offset, FPz is significantly anticorrelated with nodes of the DMN. Positive correlations with nodes of the TPN are strongest at 4 sec and later invert in sign between 16 and 20 sec. The sign inversion suggests that both the BOLD and EEG signals contain a common periodic component. Some evidence of sign inversion is also seen in the DMN at 12 sec. (Middle) Group-averaged correlation between infraslow BOLD and the FT7 electrode. Colored results are significant at FWER of 0.05. Time shifts in seconds refer to the delay imposed on the BOLD relative to EEG signals while calculating correlation. Almost no significant correlations are present in this average mapping. (Bottom) Group-averaged correlation between infraslow BOLD and the PO10 electrode. Colored results are significant at FWER of 0.05. Time shifts in seconds refer to the delay imposed on the BOLD relative to EEG signals while calculating correlation. Strong positive correlation is seen throughout gray matter between 0 and 4 sec. Between 12 and 16 sec, PO10 is anticorrelated with regions of the TPN, suggesting involvement of a periodic component that may be related to the one seen in the BOLD-FPz average. FWER, family wise error rate. Color images available online at [www.liebertpub.com/brain](http://www.liebertpub.com/brain)



the first pattern, there is then a tendency to negatively correlate with these regions at later time shifts. Thus, the two patterns bear a close spatial resemblance to one another, except that one tends to begin earlier and frequently covers larger swaths of gray matter. BOLD correlates of the remaining electrodes (PO9 and FT7) exhibited almost no significance at any shift (Fig. 5, middle).

During analysis of EEG-BOLD correlation, a large degree of variability in the correlations between trials was observed that was effectively lost during group averaging. The patterns sometimes resembled RSNs not seen in Figure 5, occasionally occurred at vastly different offsets and even negative offsets (which seem to suggest that BOLD events precede related ones in EEG), and sometimes exhibited an inversion of sign compared to the patterns that appeared in the averages.

Figure 6 provides two examples of the individual variability. Shown are the correlation mappings between BOLD and FT7 (where there was little group-level correlation) for two separate trials, which are representative of the kinds of differences that have been observed. As shown in Figure 5, the relationship between FT7 and BOLD averaged out to an almost entirely in-

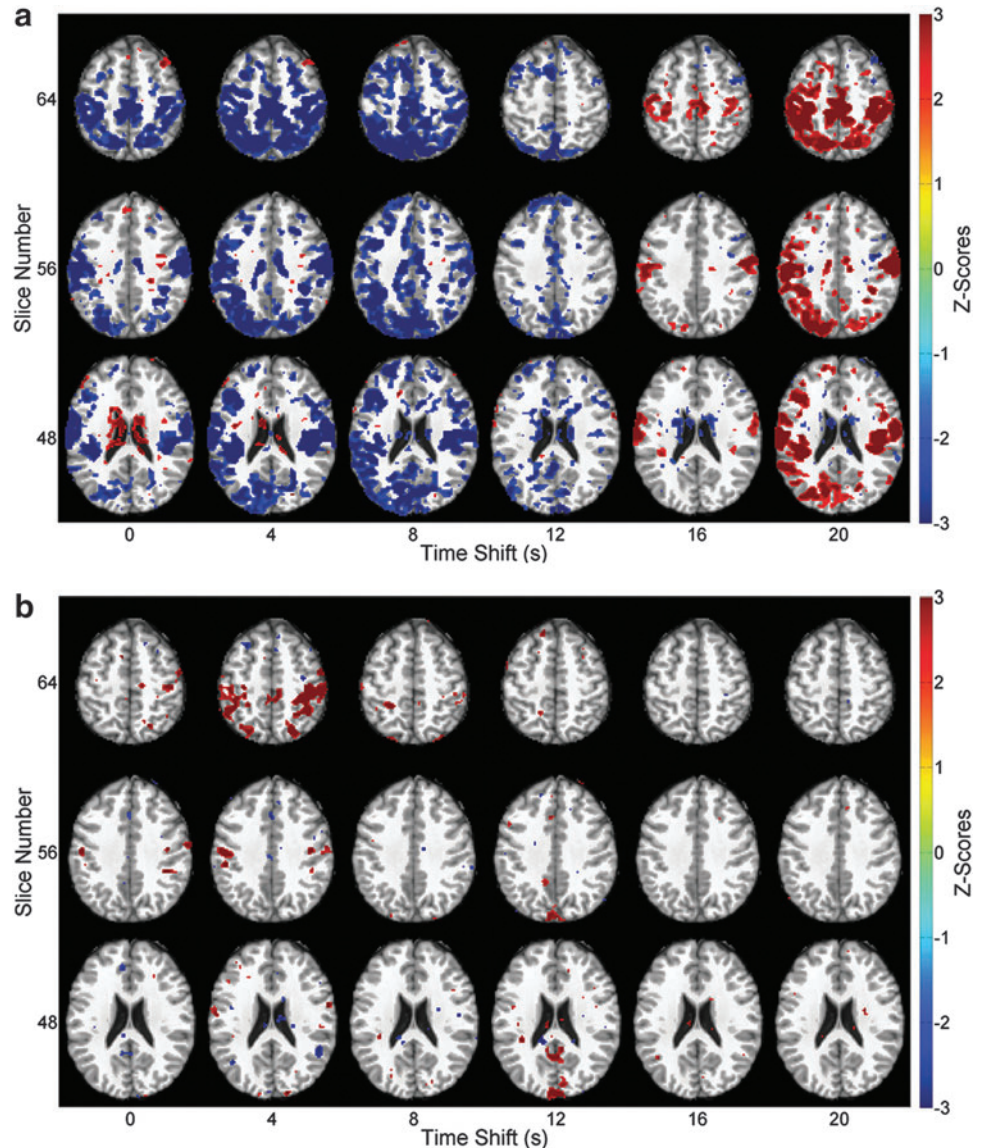
significant result. In contrast, the BOLD-FPz correlations displayed the most common tendencies (Fig. 6, bottom). Mappings for other channels typically fell between these extremes, with significant values in the group averages reflecting more consistency in the results for individual scans.

We also examined the relationship between the average signal of each RSN based on ICA and the signal from each electrode. The majority of the ICs were easily recognizable and corresponded well with known RSN topographies (Damoiseaux et al., 2006; Lee et al., 2013; Rosazza and Minati, 2011; Veer et al., 2010) or brain structures (Fig. 7). Averaged correlations between each RSN and the infraslow EEG signals tended to be weak and no values passed significance thresholding with FWER correction (data not shown).

#### Dynamic analysis

For each electrode and each trial, a series of sliding window EEG-BOLD correlation maps were created. Example videos are shown in the Supplementary Data (Supplementary Videos S1 and S2). These images were manually inspected

**FIG. 6.** (a) Single-trial correlation between infraslow BOLD and the FT7 electrode for one trial. Colored results are significant at an FWER of 0.05. Time shifts in seconds refer to the delay imposed on the BOLD relative to EEG signals while calculating correlation. (b) Single-trial correlation between infraslow BOLD and the FT7 electrode for a different trial. The pattern of correlation has little in common with the pattern observed in the first trial. (c) Single-trial correlation between infraslow BOLD and the FPz electrode for one trial. (d) Single-trial correlation between infraslow BOLD and the FPz electrode for a different trial. Despite substantial differences from the previous trial, the patterns of correlation for the two trials have several areas in common. Color images available online at [www.liebertpub.com/brain](http://www.liebertpub.com/brain)



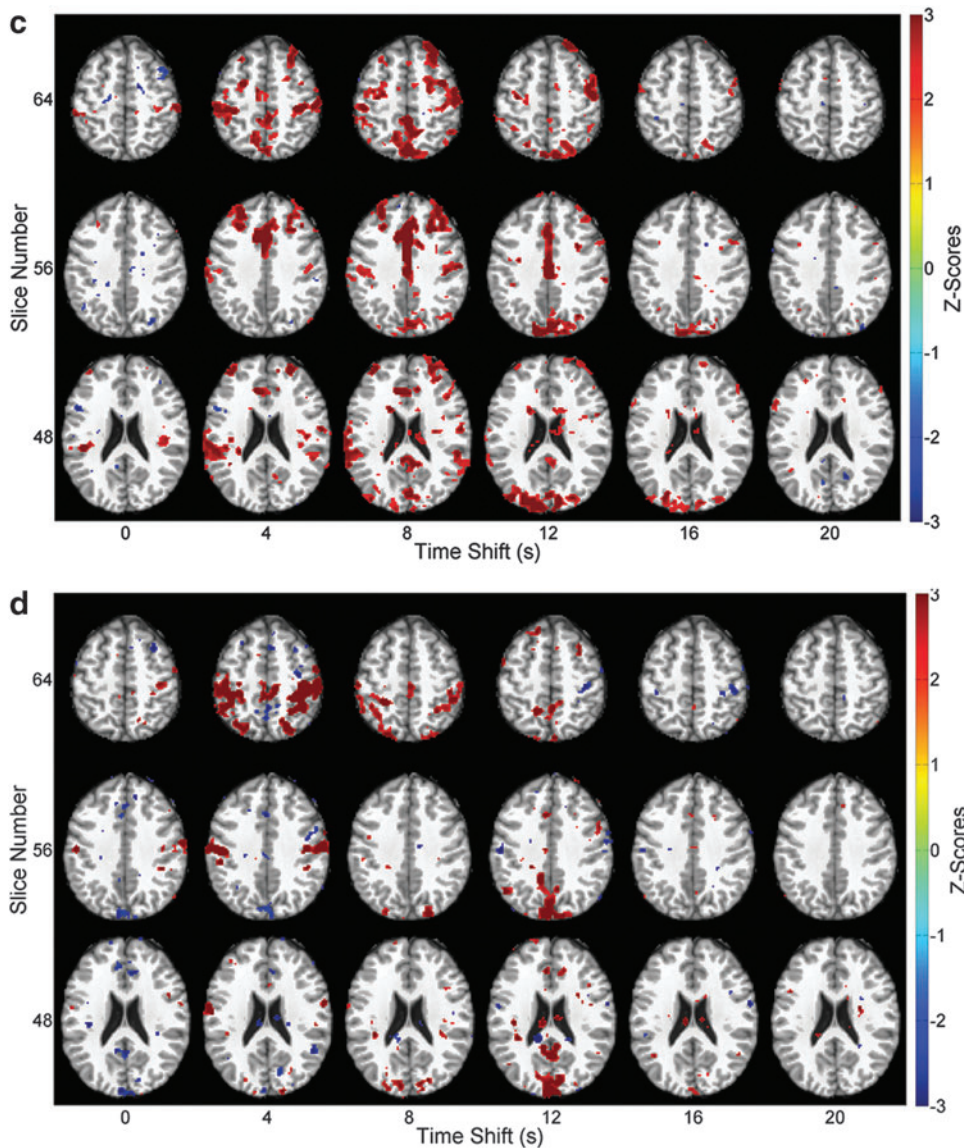
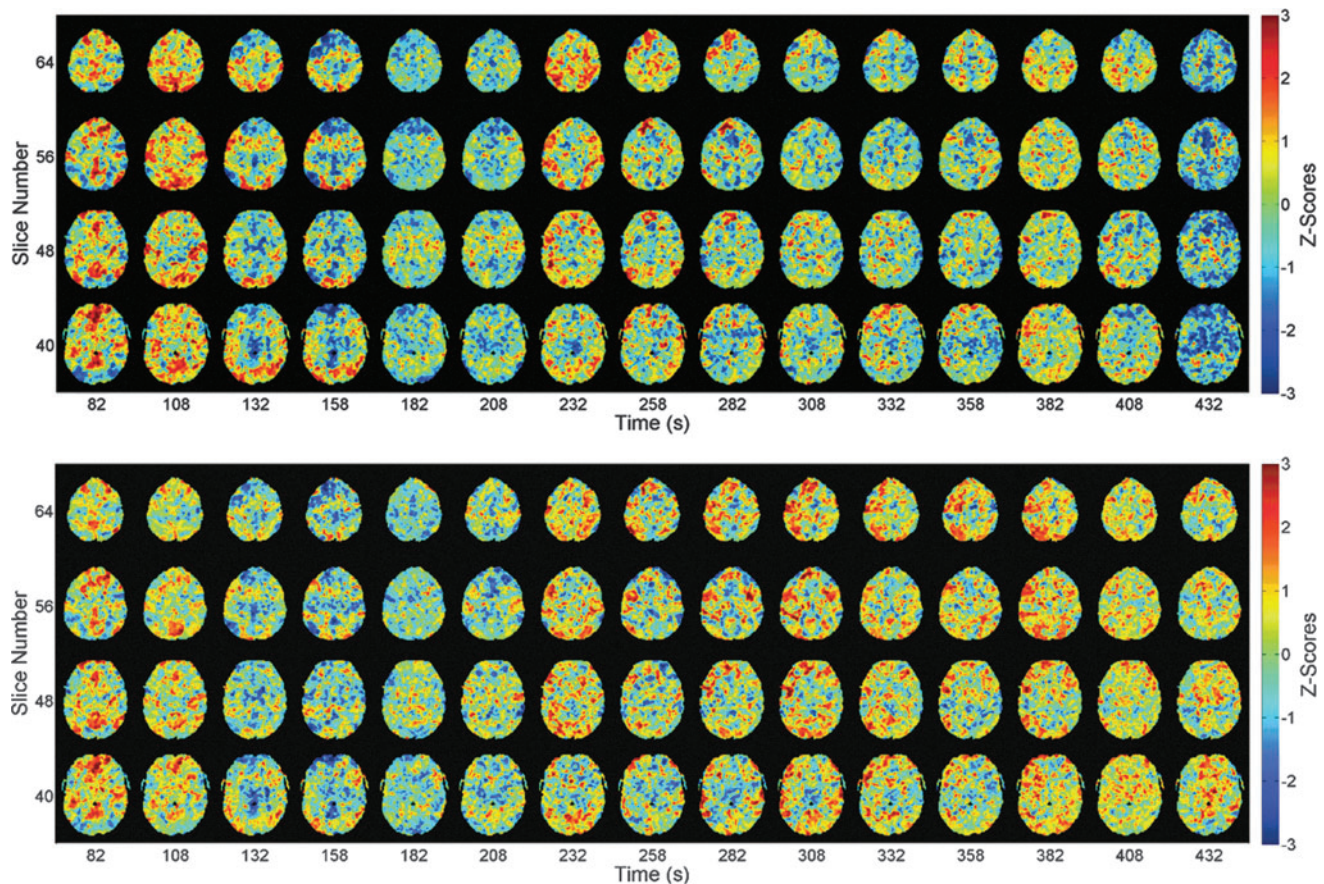


FIG. 6. (Continued).

for patterns and trends. The most prominent feature observed was the presence of strong correlation in nodes of various resting state networks. Easily the most prevalent among them are the sensorimotor cortices, the IPS of the TPN, and the various nodes of the DMN. BOLD-EEG dynamic correlations were visible in these particular nodes at multiple time points in the example images (Fig. 7). Other networks were also visible in other trials and with other seed electrodes. As suggested by the periodicity observed in the static analysis, RSN-like patterns sometimes inverted in sign over time. Other patterns emerge and disappear at multiple time points while retaining the same sign or transition between electrodes without a sign change. In at least three trials, patterns were observed to be stable for as long as 200 sec. In others, such as the example images in Figure 7, they vary much more rapidly (lasting ~25–50 sec). Varying degrees of spatial stability were also observed. Segments of correlation mappings across nearly all electrodes exhibit very similar patterns in some trials. Other trials provide examples of differing patterns across electrodes. On this last point, however, it should be noted that this tends to only be observable in

channels that are remote from one another on the electrode montage. Not surprisingly, the correlation mappings are extremely variable across trials. Any given pair of trials, even ones that originate from the same subject, are distinct. We compared the mean of the histogram of the sliding window correlation data for real and null distributions and found that the real distribution was significantly more positive ( $p < 0.01$ ).

The variability observed even for a single electrode motivated a deeper exploration of the sliding window correlation results. A recent article by Leonardi et al. (2013) showed that certain network configurations act as “building blocks” of the time course of functional connectivity between regions. We hypothesized that similar building blocks existed for the correlation time course for the EEG and BOLD data. To test this, the SWC series were decomposed using group sICA, and the resulting components were examined for resemblance to RSNs. Performing this test using the same parameters as before yielded the results in Figure 8, which do appear very similar to RSNs established in literature (Damoiseaux et al., 2006; Rosazza and Minati, 2011; Veer et al., 2010).



**FIG. 7.** Example SWC volumes over time series from one trial. Top: Dynamic correlations between infraslow BOLD and the electrode FT8. High magnitude correlations between EEG and RSN nodes are visible at multiple time shifts. Correlation with midline DMN nodes starts strongly positive at 82 sec and shifts to strongly negative at 158 sec. More lateral areas join the DMN around 258 sec. The TPN is clearest at 132 and 232 sec. It should be emphasized that these are windowed single trials from single subjects and thus noisier than typical rs-MRI data. Bottom: BOLD-TP9 SWC series from the same trial. Correlation morphologies are mostly similar to those of FT8 until  $\sim 282$  sec, where they begin to diverge appreciably. Between 308 and 382 sec, TP9 appears to correlate with lateralized components while FT8 appears uncorrelated. rs-MRI, Resting state magnetic resonance imaging. Color images available online at [www.liebertpub.com/brain](http://www.liebertpub.com/brain)

### Quasiperiodic patterns

The QPPs created using the pattern-finding algorithm were similar in appearance and timing to those described in Majeed et al. (2011). Most electrodes exhibited significant positive and negative correlation with the QPP template strength time course but maxima and minima occurred at several clusters of lag times (Fig. 9). Relative levels of positive and negative correlation for each electrode are shown in Supplementary Figure S2. The two most prominent clusters of positive correlation fell between time shifts of  $-10$  and  $-30$  sec. The two most prominent clusters of negative correlation fell between  $-20$  and  $10$  sec. As QPP phase is arbitrary, the relationship between time shifts is more important than their actual values. The alternation of the clusters is suggestive of a quasiperiodic process, as expected. The electrodes with the strongest correlation or anticorrelation were generally located in the frontal regions and tended to lead the rest of the brain (Fig. 10). These results indicate that correlates of the QPP can be observed in the DC EEG signal, in line with previous work in rats, compared to Figure 5 of Thompson et al. (2014b).

### Discussion

The simultaneous acquisition of DC-EEG and MRI in this study allowed a deeper investigation of the relationship between the spontaneous BOLD fluctuations and electrical activity in the same infraslow frequency bands. The strong, widespread, and significant correlations witnessed between BOLD and EEG across the electrodes suggest that there is indeed a direct relationship between them at infraslow frequencies. A subset of electrodes exhibited significant positive and negative correlation as a function of the time lag between the two signals. This periodic alternation was similar to the correlation observed between infraslow LFPs and the BOLD signal in the rat, where infraslow activity is closely tied to QPPs in the BOLD signal (Thompson et al., 2014b; Pan et al., 2013). QPP strength over time was also correlated to the signal from some electrodes, particularly frontal electrodes. Together these suggest that the relationship between QPPs and infraslow activity in the rat is also present in the human. A closer investigation of the time-varying relationship between DC-EEG and BOLD found that the relationship varied substantially even over a single

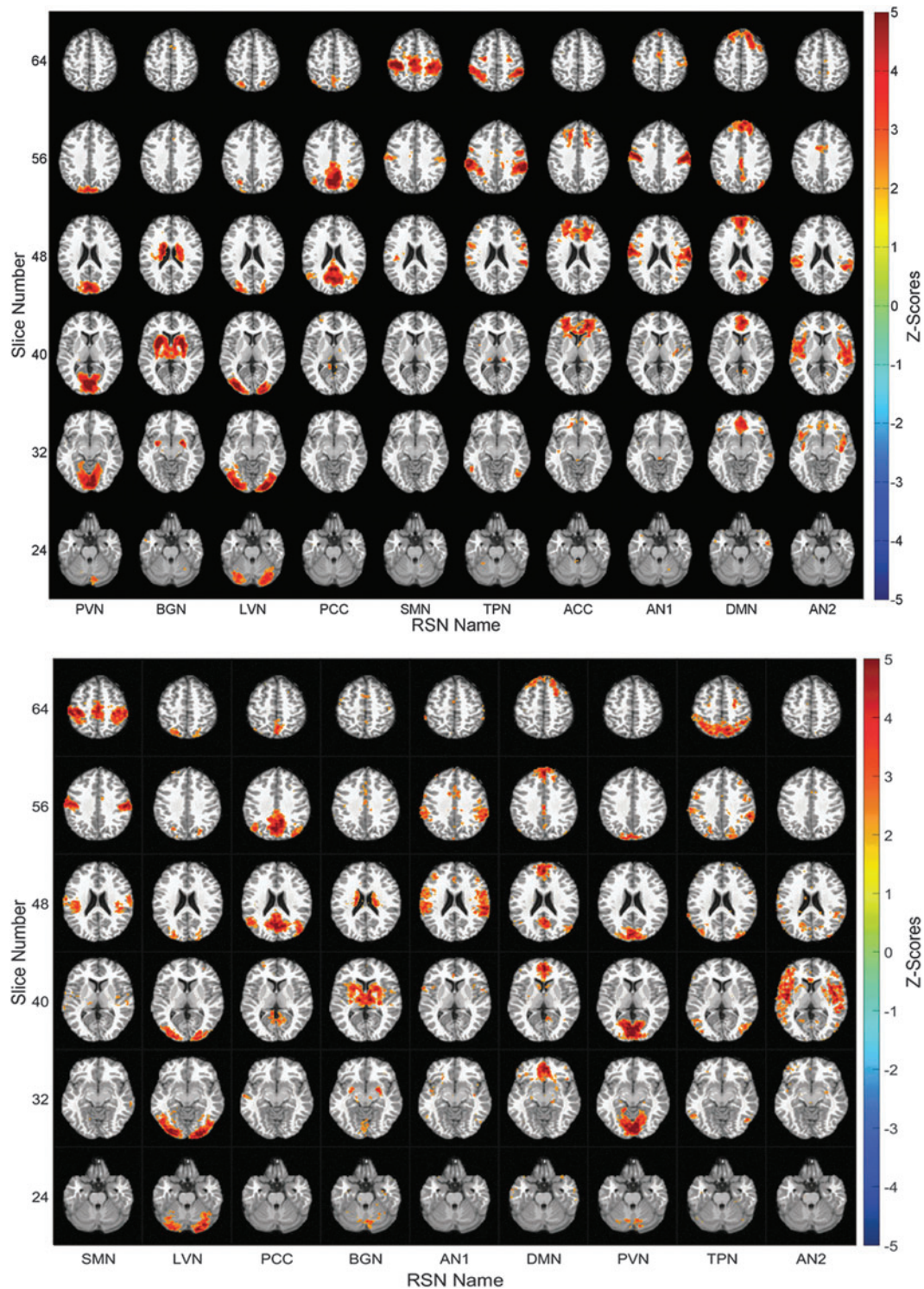


**FIG. 8.** (Top) Independent spatial components of the resting state BOLD data. Out of 20 total components, the 10 are shown here and are labeled along the horizontal axis with the following acronyms: primary visual (PVN), basal ganglia (BGN), lateral visual (LVN), posterior cingulate cortex (PCC), sensorimotor (SMN), task positive network (TPN), anterior cingulate cortex (ACC), first auditory (AN1), default mode (DMN), and second auditory (AN2). (Bottom) An example of the independent spatial components of BOLD-EEG SWC series. Group sICA decomposes the correlation volumes into components that strongly resemble RSNs, consistent with the notion that RSNs are coherent units of the infraslow BOLD-EEG coupling. Other networks, including lateralized, salience, and precuneus components, were also present but are not shown. Substantial similarity is present compared to the ICs created from the BOLD signal alone. Color images available online at [www.liebertpub.com/brain](http://www.liebertpub.com/brain)

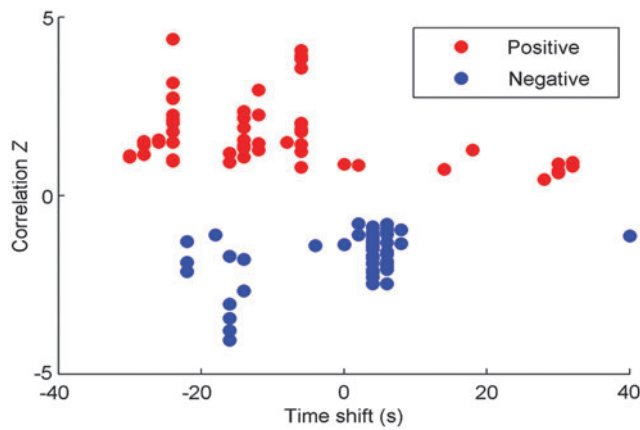


**FIG. 9.** Two dots are shown for each electrode, a red dot for the time shift and value of the maximum correlation between QPP strength over time and the DC-EEG signal and a blue dot for the minimum correlation. Nonsignificant electrodes are not shown. Two substantial positive clusters (approximately  $-25$  and  $-10$  sec) and two negative clusters (approximately  $-15$  and  $5$  sec) are present. Clusters appear to be separated by  $\sim 20$  sec, on the time scale of the QPPs and in line with the periodicity of the correlation between EEG and BOLD observed in some electrodes. This demonstrates that correlates of the QPP can be observed in the DC-EEG signal and that several clusters of significant time points exist. Color images available online at [www.liebertpub.com/brain](http://www.liebertpub.com/brain)

scan. The patterns of correlation had a qualitative resemblance to resting state networks, which motivated us to apply ICA to the sliding window time courses. The results showed that correlation between BOLD and EEG seems to arise through combinations of resting state networks.

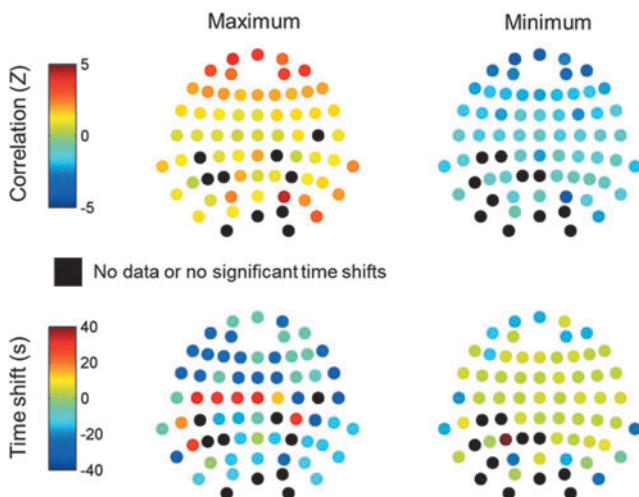


**FIG. 10.** EEG spatial map of the data shown in Figure 9. Alignment is as in Figure 1. (Top row) Maximum and minimum correlation between DC-EEG in each electrode and QPP strength over time (whole brain). (Bottom row) Time shift where maximum and minimum correlation occurred. The highest correlation with QPP strength is in frontal and occipital electrodes. The time shift patterns are less clear, but especially for the maximum correlations, there appear to be several domains of time shifts with distinct locations on the scalp. This suggests that the QPP measured with MRI may reflect shifting electrical potentials. Color images available online at [www.liebertpub.com/brain](http://www.liebertpub.com/brain)

### Previous studies linking infraslow electrical activity and MRI

A number of researchers have speculated about the existence of an infraslow electrophysiological counterpart to BOLD signals (Drew et al., 2008; He et al., 2008; Palva and Palva, 2012). A considerable body of indirect evidence exists to suggest such a mechanism (for a review, see Palva and Palva, 2012). The most direct evidence for a relationship between the two came from studies in the anesthetized rat (Pan et al., 2013). Significant temporal correlations were observed between simultaneously recorded BOLD and infraslow LFP signals, indicating that the two signals are indeed closely related. Correlations were well localized to cortical tissue and observed at signal delays approximating the hemodynamic response interval, which is consistent with the notion of a causal relationship between electrophysiology and hemodynamics. Interestingly, further work in the rodent showed that the pattern of infraslow LFP-BOLD correlation closely mimicked the QPPs of BOLD fluctuations observed with MRI alone, suggesting that these patterns may reflect coordinated infraslow oscillations (Thompson et al., 2013, 2014a, 2014b, 2015).

Simultaneously recorded BOLD and EEG data also found a relationship between infraslow activity and the BOLD signal (Hiltunen et al., 2014). They found that the ICs of the envelope of the full-band EEG are correlated with BOLD in spatial patterns that match the signatures of well-known functional networks in resting humans, lending strong support to the hypothesis that, at least, in part, functional connectivity arises from equivalently slow electrophysiological activity. Our study also found patterns of BOLD-EEG correlation that match commonly observed resting state networks, particularly in the TPN. Furthermore, nodes of the DMN (Buckner et al., 2008; Raichle et al., 2001) are visible in the BOLD-FPz mappings (Fig. 5, top) and display a significant anticorrelated relationship. A following study by Korhonen et al. (2014) also found considerable variability in the correlation between the EEG components and the BOLD signal over time, in agreement with our results.

### Behavioral and physiological relevance of infraslow activity

Although the majority of EEG-related studies do not examine signals below 1 Hz, their existence has nevertheless been documented for many years in both humans (Monto et al., 2008; Trimmel et al., 1990; Vanhatalo et al., 2005) and animals (Aladjalova, 1957; Filippov et al., 2002; Pan et al., 2013). Evidence shows that spontaneous waveforms at these frequencies are a feature of recordings made in preterm neonates (Vanhatalo et al., 2002, 2005) and in sleeping adults (Vanhatalo et al., 2004, 2005). They have also been linked to both task performance (Monto et al., 2008; Trimmel et al., 1990, 2001) and attentional disorders (Helps et al., 2008, 2009, 2010). It has also been found that the phases of infraslow fluctuations are well-correlated with the amplitudes of faster activity (Aladjalova, 1957; Monto et al., 2008; Vanhatalo et al., 2004). This phenomenon is an example of *phase-amplitude* or *cross-frequency coupling* (Canolty and Knight, 2010), a topic that has been gaining increasing attention in the study of brain networks. Such a relationship between the EEG bands suggests that infraslow activity could be reflecting large-scale cortical excitability (Elbert, 1993). Alternately, localized infraslow oscillators may drive

both electrical potentials and local oxygenation (Li et al., 2015) or astrocytic or neural mitochondrial calcium signals may play a critical role (Jego et al., 2015; Sanganahalli et al., 2013). Using invasive electrophysiology in rat models, Thompson et al. (2014b and 2015) provided evidence that fast and infraslow local field potentials contribute differently to spontaneous BOLD fluctuations and dynamics, although this does not rule out coupling between the frequencies. If the infraslow frequencies do contain independent information, infraslow EEG may provide key insights about functional connectivity.

#### *Evidence of QPPs*

In the static correlation analysis, most electrodes demonstrate positive correlation at some temporal offsets and negative correlation at others. Occasionally more than one cycle is observed. These effects are particularly pronounced in areas of the TPN such as sensorimotor cortex (Fig. 5 top shows a strong example; weaker effects can be seen in Fig. 5 bottom). The time between peak positive correlation and peak negative correlation is  $\sim 10$  sec. The alternation between positive and negative correlation suggests a periodic process (like the QPP) and is similar to the pattern of correlation between BOLD and infraslow activity observed in rats (Pan et al., 2013). In addition, the timing between the positive and negative correlation is approximately half the length of the QPP in humans. These data strongly suggest that the QPPs in humans have a similar relationship to infraslow activity as those observed in rats. The link between infraslow activity and QPPs is confirmed more directly by the strong periodic patterns of correlation observed between the QPP template strength time course and the DC EEG signal.

#### *Variability of the relationship between BOLD and infraslow EEG*

The variability that was found between trials and across the various analysis parameters highlights the potential complexity of the infraslow BOLD-EEG relationship. In particular, it seems that their coupling is temporally dynamic, or capable of changing across time, because analyses of separate trials from the same individual typically yielded inconsistent results. This finding may be related to similarly high intertrial variability that has been observed in other simultaneous fMRI-EEG studies investigating higher frequency ( $>1$  Hz) electrophysiology (Gonçalves et al., 2006; Meyer et al., 2013).

Part of the variability may arise from the relatively uncertain spatial origins of the infraslow EEG signals. Even if volume conduction is not a contributing factor as suggested in Khader et al. (2008), the EEG records a mixture of electrical activity across cortical regions of unknown size and overlap. This is a problem that is inherent to working in electrode space as opposed to brain space (Laufs et al., 2008). As regional measures, EEG signals are biased toward capturing the larger scale, most proximal, and most active networks at any given time. Contributions from less active, smaller scale, and deeper networks are probably obscured to varying degrees in the recordings. The configuration of active brain networks can change substantially over brief intervals, which is likely to have complicated effects on EEG readings. It is therefore plausible that some nonstationarities in their relationship arise from the low spatial resolution and lack of depth information in EEG, meaning that common components between the infraslow signals may change because

scalp electrophysiology only reflects a dominant subset of network activity per time point. Source reconstruction might provide a better estimation of the localized relationship between BOLD and DC EEG. However, it would be far from trivial, given that the source model would be complex, widespread, difficult to predefine, and signal-to-noise ratio perhaps suboptimal.

It is also likely that infraslow EEG by itself cannot completely characterize the overall BOLD-EEG relationship. Others have noted evidence that the BOLD signal contains information related to multiple frequency bands of neuronal activity (Chang et al., 2013; Keilholz, 2014; Laufs et al., 2006; Magri et al., 2012; Mantini et al., 2007; Meyer et al., 2013; Raichle, 2011) and that these different bands might coordinate activities across different distances (Buzsáki, 2006).

#### *RSNs as building blocks of the infraslow EEG signal*

An interesting aspect of the variability observed in the correlation between DC EEG and BOLD both across trials and within a single trial (using SWC) was the presence of correlation patterns that resembled resting state networks. The particular network that correlated with a given electrode sometimes changed over time, indicating that there is not a simple one-to-one mapping. Further analysis of the sliding window time course using ICA suggests that the patterns of time-varying correlation are combinations of common resting state networks. Taken together with the results from the Hiltunen et al. study, this suggests that each network may have an infraslow signature, and the DC EEG signal at the surface of the scalp can be dominated by different networks as their relative levels of activity change over time. QPPs may then account for some of the temporal variability of which network dominates, manifesting as a large-scale modulation of the DMN and TPN in particular. In this case, the DC-EEG and BOLD signals may both represent multiple spatial and temporal scales of activity within the brain.

#### *Limitations and future directions*

Our ability to interpret the results of this study is somewhat limited by a general lack of knowledge about infraslow EEG. While infraslow EEG correlates with BOLD signals derived from cortical gray matter, it is difficult to disentangle the non-neuronal and neuronal contributors to this correlation. Infraslow EEG, in particular, is susceptible to contributions from numerous sources, including variations in  $\text{CO}_2$  concentrations (Voipio et al., 2003) and blood volume (Vanhatalo et al., 2003), which can also contribute to the BOLD signal. Further work in the animal model may help to unravel some of the sources of the infraslow oscillations.

Most EEG studies do not examine infraslow activity. To record very slow activity with high fidelity, special constraints on preparation and hardware are required (Khader et al., 2008; Tallgren, 2006; Tallgren et al., 2005; Vanhatalo et al., 2005). A DC-capable amplifier with high input impedance and wide dynamic range is needed, especially when recording over longer intervals. Many EEG amplifiers are AC-coupled and are, therefore, incapable of accurately recording long segments of nearly constant potential (Bauer et al., 1989). Furthermore, nonpolarizable Ag/AgCl electrodes and a chloride-containing gel are required (Tallgren et al., 2005), which precludes nearly all alternative electrode materials and electrolyte-free gels. Finally, special considerations must be made for the galvanic skin response, which can introduce

artifacts that are indistinguishable from neuronal activity (Birbaumer et al., 1990). This entails abrading the scalp beneath each electrode recording site (Vanhatalo et al., 2005). Despite these obstacles, the correlation observed between infraslow activity and the BOLD signal insures that at least some of the DC EEG signal has a neurophysiological origin. The fact that correlations are localizable to gray matter and RSN-like topographies provides some indication that they result from neuronal activity. Extensive work has gone into successfully linking BOLD RSNs to behavior (for reviews, see Rosazza and Minati, 2011; van den Heuvel and Hulshoff Pol, 2010), and the tendency of BOLD-EEG correlations to feature these networks is a clue that they too could be behaviorally relevant. In addition, and perhaps relatedly, infraslow EEG signals have been linked to similar behaviors (Helps et al., 2009; Monto et al., 2008).

The sliding-window correlation analysis has a number of pitfalls that complicate the interpretation of its results. The choice of window length can have a profound impact on results (Keilholz et al., 2013; Leonardi and Van De Ville, 2015; Thompson et al., 2013c), and a method of determining an “ideal” length is not currently known (Shakil et al., 2016). There is also contention whether windowed connectivity measures a dynamic process versus a shorter portion of a static process (Hindriks et al., 2016). In addition, testing SWC signals for statistical significance can be difficult. Data preprocessing in general has been known to impose correlations both within and between signals and can thereby sharply reduce the degrees of freedom in the data. The permutation tests used for this study were applied to identically processed data and should provide a strict control against false positives. The statistical analysis of the sliding window correlation data is the most challenging portion of the study. Ideally, all possible permutations of the data would be piped into ICA, and the amount of variance that each component explained, their spatial resemblance to RSNs, and the amount of time that they were active during the scan would all be calculated and compared to the real data. We hope to tackle this problem in the future when we have greater computational power. In the mean time, however, we believe that showing that the means of the sliding window correlations are significantly more positive for real data than for null data shows that the BOLD fluctuations do reflect at least a portion of the EEG signal in a meaningful way.

The sliding window correlation analysis assumed a time lag between BOLD and EEG of 4 sec, based on similar hemodynamic delays measured during task-based activity. However, there are indications that the hemodynamic response function for resting state MRI is somewhat different than would be expected for task-based fMRI (Chen and Glover, 2015) and it is possible that the time lag of 4 sec is not ideal. This issue only affects the sliding window correlation, as analysis was performed for a range of lags for the static correlation. In our previous work in rodents, we found the hemodynamic delay for resting state MRI to be very similar to the hemodynamic delays for task-based fMRI under the same anesthetic (Pan et al., 2011, 2013).

The results of this study show that infraslow electrical activity is intricately involved in the coordination of BOLD fluctuations that make up functional networks. Its role in attention and the close links observed to QPPs, the DMN, and the TPN all suggest that infraslow activity plays a role in large-scale processes involved in external versus internal orientation. Alterations of DMN connectivity, in particular, have been observed in numerous disorders and may be tied to changes in

infraslow activity as well. Moreover, its contribution to the BOLD signal suggests that the multiscale structure of the brain is reflected at least to some extent in the BOLD fluctuations, motivating efforts to find ways to separate and analyze specific components of the BOLD signal to improve sensitivity to brain dysfunction and cognitively relevant activity.

### Acknowledgments

This work was supported by the Air Force Center of Excellence (BIONIC) at Georgia Tech and NIH R01NS078095. Garth Thompson was supported by the Department of Homeland Security fellowship and NIH fellowship 2T32DA022975-06A1. The DC -EEG system was generously loaned to us by the Atlanta VAMC Rehabilitation Research and Development Center. The authors thank Frank Diebel and Nytavia Wallace for their technical assistance in data recording.

### Author Disclosure Statement

No competing financial interests exist.

### References

- Aguirre GK, Zarahn E, D’Esposito M. 1997. Empirical analyses of BOLD fMRI statistics. *Neuroimage* 5:199–212.
- Aladjalova NA. 1957. Infra-slow rhythmic oscillations of the steady potential of the cerebral cortex. *Nature* 179:957–959.
- Bauer H, Korunka C, Leodolter M. 1989. Technical requirements for high-quality scalp DC recordings. *Electroencephalogr Clin Neurophysiol* 72:545–547.
- Bell AJ, Sejnowski TJ. 1995. Information-maximization approach to blind separation and blind deconvolution. *Neural Comput* 7:1129–1159.
- Birbaumer N, Elbert T, Canavan AG, Rockstroh B. 1990. Slow potentials of the cerebral cortex and behavior. *Physiol Rev* 70:1–41.
- Buckner RLL, Andrews-Hanna JRR, Schacter DLL. 2008. The brain’s default network: anatomy, function, and relevance to disease. *Ann N Y Acad Sci* 1124:1–38.
- Buzsáki G. 2006. *Rhythms of the Brain*. New York: Oxford University Press.
- Calhoun VD, Adali T, Pearlson GD, Pekar JJ. 2001. A method for making group inferences from functional MRI data using independent component analysis. *Hum Brain Mapp* 14:140–151.
- Canolty RT, Knight RT. 2010. The functional role of cross-frequency coupling. *Trends Cogn Sci* 14:506–515.
- Carvajal-Rodríguez A, de Una-Alvarez J, Rolán-Alvarez E, Carvajal-Rodríguez A, de Uña-Alvarez J, Rolán-Alvarez E. 2009. A new multitest correction (SGoF) that increases its statistical power when increasing the number of tests. *BMC Bioinformatics* 10:209.
- Chang C, Glover GHH. 2010. Time-frequency dynamics of resting-state brain connectivity measured with fMRI. *Neuroimage* 50:81–98.
- Chang C, Liu Z, Chen MCC, Liu X, Duyn JHH. 2013. EEG correlates of time-varying BOLD functional connectivity. *Neuroimage* 72:227–236.
- Chen JE, Glover GH. 2015. BOLD fractional contribution to resting-state functional connectivity above 0.1 Hz. *Neuroimage* 107:207–218.
- Cox RW. 1996. AFNI: software for analysis and visualization of functional magnetic resonance neuroimages. *Comput Biomed Res* 29:162–173.
- Damoiseaux JS, Rombouts SARB, Barkhof F, Scheltens P, Stam CJ, Smith SM, Beckmann CF, 2006. Consistent resting-state

- networks across healthy subjects. *Proc Natl Acad Sci U S A* 103:13848–13853.
- Davey CE, Grayden DB, Egan GF, Johnston LA. 2013. Filtering induces correlation in fMRI resting state data. *Neuroimage* 64:728–740.
- Delorme A, Makeig S. 2004. EEGLAB: an open source toolbox for analysis of single-trial EEG dynamics including independent component analysis. *J Neurosci Methods* 134:9–21.
- Dinges DFF, Powell JWW. 1985. Microcomputer analyses of performance on a portable, simple visual Rt task during sustained operations. *Behav Res Methods Instruments Comput* 17:652–655.
- Drew PJJ, Duyn JHH, Golanov E, Kleinfeld D. 2008. Finding coherence in spontaneous oscillations. *Nat Neurosci* 11: 991–993.
- Elbert T. 1993. Slow cortical potentials reflect the regulation of cortical excitability. In: McCallum WC, Curry SH (eds.) *Slow Potential Changes in the Human Brain*. New York: Plenum Pub. Corp.; pp. 235–251.
- Filippov IV, Gladyshev AV, Williams WC. 2002. Role of infraslow (0–0: 5 Hz) potential oscillations in the regulation of brain stress response by the locus coeruleus system. *Neurocomputing* 46:795–798.
- Fisher RA. 1915. Frequency distribution of the values of the correlation coefficient in samples from an indefinitely large population. *Biometrika*. DOI:10.2307/2331838
- Fox MDD, Snyder AZZ, Vincent JLL, Corbetta M, Van Essen DCC, Raichle MEE. 2005. The human brain is intrinsically organized into dynamic, anticorrelated functional networks. *Proc Natl Acad Sci U S A* 102:9673–9678.
- Fransson P. 2005. Spontaneous low-frequency BOLD signal fluctuations: an fMRI investigation of the resting-state default mode of brain function hypothesis. *Hum Brain Mapp* 26:15–29.
- Gonçalves SI, de Munck JC, Pouwels PJW, Schoonhoven R, Kuijter JPA, Maurits NM, et al. 2006. Correlating the alpha rhythm to BOLD using simultaneous EEG/fMRI: inter-subject variability. *Neuroimage* 30:203–213.
- Grigg O, Grady CLL. 2010. Task-related effects on the temporal and spatial dynamics of resting-state functional connectivity in the default network. *PLoS One* 5:e13311.
- Handwerker DA, Roopchansingh V, Gonzalez-Castillo J, Bandettini PA. 2012. Periodic changes in fMRI connectivity. *Neuroimage* 63:1712–1719.
- He BJJ, Snyder AZZ, Zempel JMM, Smyth MDD, Raichle MEE. 2008. Electrophysiological correlates of the brain’s intrinsic large-scale functional architecture. *Proc Natl Acad Sci U S A* 105:16039–16044.
- Helps S, James C, Debener S, Karl A, Sonuga-Barke EJS. 2008. Very low frequency EEG oscillations and the resting brain in young adults: a preliminary study of localisation, stability and association with symptoms of inattention. *J Neural Transm* 115:279–285.
- Helps SK, Broyd SJ, James CJ, Karl A, Sonuga-Barke EJS. 2009. The attenuation of very low frequency brain oscillations in transitions from a rest state to active attention. *J Psychophysiol* 23:191–198.
- Helps SKK, Broyd SJJ, James CJJ, Karl A, Chen W, Sonuga-Barke EJSJ. 2010. Altered spontaneous low frequency brain activity in attention deficit/hyperactivity disorder. *Brain Res* 1322:134–143.
- Hiltunen T, Kantola J, Abou Elseoud A, Lepola P, Suominen K, Starck T, et al. 2014. Infra-slow EEG fluctuations are correlated with resting-state network dynamics in fMRI. *J Neurosci* 34:356–362.
- Hindriks R, Adhikari MH, Murayama Y, Ganzetti M, Mantini D, Logothetis NK, Deco G. 2015. Can sliding-window correlations reveal dynamic functional connectivity in resting-state fMRI? *Neuroimage* 127: 242–256.
- Hutchison RM, Womelsdorf T, Gati JS, Everling S, Menon RS. 2013. Resting-state networks show dynamic functional connectivity in awake humans and anesthetized macaques. *Hum Brain Mapp* 34:2154–2177.
- Jego P, Pacheco-Torres J, Araque A, Canals S. 2014. Functional MRI in mice lacking IP3-dependent calcium signaling in astrocytes. *J Cereb Blood Flow Metab* 34: 1599–1603.
- Keilholz SD. 2014. Review article: the neural basis of time-varying resting state functional connectivity. *Brain Connect* 4:1–32.
- Keilholz SD, Magnuson ME, Pan WJ, Willis M, Thompson GJ. 2013. Dynamic properties of functional connectivity in the rodent. *Brain Connect* 3:31–40.
- Khader P, Schicke T, Röder B, Rösler F. 2008. On the relationship between slow cortical potentials and BOLD signal changes in humans. *Int J Psychophysiol* 67:252–261.
- Kim S-G, Bandettini PA. 2010. Principles of Functional MRI. In: Faro S, Mohamed F (eds.) *BOLD fMRI: A Guide to Functional Imaging for Neuroscientists*. New York: Springer-Verlag; pp. 3–22.
- Korhonen V, Hiltunen T, Myllylä T, Wang X, Kantola J, Nikkinen J, et al. 2014. Synchronous multiscale neuroimaging environment for critically sampled physiological analysis of brain function: hepta-scan concept. *Brain Connect* 4:677–689.
- Laufs H, Daunizeau J, Carmichael DW, Kleinschmidt A. 2008. Recent advances in recording electrophysiological data simultaneously with magnetic resonance imaging. *Neuroimage* 40:515–528.
- Laufs H, Holt JL, Elfont R, Krams M, Paul JS, Krakow K, Kleinschmidt A. 2006. Where the BOLD signal goes when alpha EEG leaves. *Neuroimage* 31:1408–1418.
- Lee MH, Smyser CD, Shimony JS. 2013. Resting-state fMRI: a review of methods and clinical applications. *Am J Neuroradiol* 34:1866–1872.
- Lenoski B, Baxter LC, Karam LJ, Maisog J, Debbins J. 2008. On the performance of autocorrelation estimation algorithms for fMRI analysis. *IEEE J Sel Top Signal Process* 2:828–838.
- Leonardi N, Richiardi J, Gschwind M, Simioni S, Annoni J-M, Schluep M, et al. 2013. Principal components of functional connectivity: a new approach to study dynamic brain connectivity during rest. *Neuroimage* 83:937–950.
- Leonardi N, Van De Ville D. 2015. Erratum to “On spurious and real fluctuations of dynamic functional connectivity during rest.” *Neuroimage* 104:430–436.
- Li JM, Bentley WJ, Snyder AZ, Raichle ME, Snyder LH. 2015. Functional connectivity arises from a slow rhythmic mechanism. *Proc Natl Acad Sci U S A* 112:1419837112.
- Liu X, Duyn JHH. 2013. Time-varying functional network information extracted from brief instances of spontaneous brain activity. *Proc Natl Acad Sci U S A* 110:4392–4397.
- Logothetis NK, Pauls J, Augath M, Trinath T, Oeltermann A. 2001. Neurophysiological investigation of the basis of the fMRI signal. *Nature* 412:150–157.
- Lu H, Zuo Y, Gu H, Waltz JA, Zhan W, Scholl CA, et al. 2007. Synchronized delta oscillations correlate with the resting-state functional MRI signal. *Proc Natl Acad Sci U S A* 104:18265–18269.
- Magri C, Schridde U, Murayama Y, Panzeri S, Logothetis NKK. 2012. The Amplitude and timing of the BOLD signal reflects the relationship between local field potential power at different frequencies. *J Neurosci* 32:1395–1407.
- Majeed W, Magnuson M, Hasenkamp W, Schwarb H, Schumacher EHH, Barsalou L, Keilholz SDD. 2011. Spatiotemporal dynamics

- of low frequency BOLD fluctuations in rats and humans. *Neuroimage* 54:1140–1150.
- Majeed W, Magnuson M, Keilholz SD. 2009. Spatiotemporal dynamics of low frequency fluctuations in BOLD fMRI of the rat. *J Magn Reson Imag* 30:384–393.
- Mantini D, Perrucci MG, Del Gratta C, Romani GL, Corbetta M. 2007. Electrophysiological signatures of resting state networks in the human brain. *Proc Natl Acad Sci U S A* 104:13170–13175.
- Meyer MC, van Oort ESB, Barth M. 2013. Electrophysiological correlation patterns of resting state networks in single subjects: a combined EEG–fMRI Study. *Brain Topogr* 26:98–109.
- Miezin FM, Maccotta L, Ollinger JM, Petersen SE, Buckner RL. 2000. Characterizing the hemodynamic response: effects of presentation rate, sampling procedure, and the possibility of ordering brain activity based on relative timing. *Neuroimage* 11:735–759.
- Monto S, Palva S, Voipio J, Palva JM. 2008. Very slow EEG fluctuations predict the dynamics of stimulus detection and oscillation amplitudes in humans. *J Neurosci* 28:8268–8272.
- Moosmann M, Schönfelder VH, Specht K, Scheeringa R, Nordby H, Hugdahl K. 2009. Realignment parameter-informed artefact correction for simultaneous EEG–fMRI recordings. *Neuroimage* 45:1144–1150.
- Niazy RK, Beckmann CF, Lannetti GD, Brady JM, Smith SM. 2005. Removal of FMRI environment artifacts from EEG data using optimal basis sets. *Neuroimage* 28:720–737.
- Palva JM, Palva S. 2012. Infra-slow fluctuations in electrophysiological recordings, blood-oxygenation-level-dependent signals, and psychophysical time series. *Neuroimage* 62:2201–2211.
- Pan W-J, Thompson G, Magnuson M, Majeed W, Jaeger D, Keilholz S. 2011. Broadband local field potentials correlate with spontaneous fluctuations in functional magnetic resonance imaging signals in the rat somatosensory cortex under isoflurane anesthesia. *Brain Connect* 1:119–131.
- Pan W-JJ, Thompson GJ, Magnuson ME, Jaeger D, Keilholz S. 2013. Infralow LFP correlates to resting-state fMRI BOLD signals. *Neuroimage* 74:288–297.
- Poldrack RA, Mumford JA, Nichols TE. 2011. *Handbook of Functional MRI Data Analysis*. New York: Cambridge University Press.
- Raichle ME. 2011. The restless brain. *Brain Connect* 1:3–12.
- Raichle ME, MacLeod AM, Snyder AZ, Powers WJ, Gusnard DA, Shulman GL. 2001. A default mode of brain function. *Proc Natl Acad Sci U S A* 98:676–682.
- Rosazza C, Minati L. 2011. Resting-state brain networks: literature review and clinical applications. *Neurol Sci* 32:773–785.
- Sakoğlu Ü, Pearson GD, Kiehl Ka, Wang YM, Michael AM, Calhoun VD. 2010. A method for evaluating dynamic functional network connectivity and task-modulation: application to schizophrenia. *Magn Reson Mater Physics Biol Med* 23:351–366.
- Sanganahalli BG, Herman P, Hyder F, Kannurpatti SS, Lutsep H. 2013. Mitochondrial Functional State Impacts Spontaneous Neocortical Activity and Resting State fMRI. *PLoS One* 8: e63317.
- Shakil S, Lee CH, Keilholz SD. 2016. Evaluation of sliding window correlation performance for characterizing dynamic functional connectivity and brain states. *Neuroimage* 133: 111–128.
- Shmuel A, Leopold DA. 2008. Neuronal correlates of spontaneous fluctuations in fMRI signals in monkey visual cortex: implications for functional connectivity at rest. *Hum Brain Mapp* 29:751–761.
- Stam CJ, Nolte G, Daffertshofer A. 2007. Phase lag index: assessment of functional connectivity from multi channel EEG and MEG with diminished bias from common sources. *Hum Brain Mapp* 28:1178–1193.
- Tallgren P, Vanhatalo S, Kaila K, Voipio J. 2005. Evaluation of commercially available electrodes and gels for recording of slow EEG potentials. *Clin Neurophysiol* 116:799–806.
- Thompson GJ, Merritt MD, Pan WJ, Magnuson ME, Grooms JK, Jaeger D, Keilholz SD. 2013. Neural correlates of time-varying functional connectivity in the rat. *Neuroimage* 83:826–836.
- Thompson GJ, Pan W-J, Billings JCW, Grooms JKK, Shakil S, Jaeger D, Keilholz SD. 2014a. Phase-amplitude coupling and infralow (<1 Hz) frequencies in the rat brain: relationship to resting state fMRI. *Front Integr Neurosci* 8:41.
- Thompson GJ, Pan W-J, Keilholz SD. 2015. Different dynamic resting state fMRI patterns are linked to different frequencies of neural activity. *J Neurophysiol* 114:114–124.
- Thompson GJ, Pan WJ, Magnuson ME, Jaeger D, Keilholz SD. 2014b. Quasi-periodic patterns (QPP): large-scale dynamics in resting state fMRI that correlate with local infralow electrical activity. *Neuroimage* 84:1018–1031.
- Thompson GJ, Riedl V, Grimmer T, Drzezga A, Herman P, Hyder F. 2016. The whole-brain “Global” signal from resting state fMRI as a potential biomarker of quantitative state changes in glucose metabolism. *Brain Connect*. DOI:10.1089/brain.2015.0394
- Trimmel M, Mikowitsch A, Groll-Knapp E, Haider M. 1990. Occurrence of infralow potential oscillations in relation to task, ability to concentrate and intelligence. *Int J Psychophysiol* 9:167–170.
- Trimmel M, Strässler F, Knerer K. 2001. Brain DC potential changes of computerized tasks and paper/pencil tasks. *Int J Psychophysiol* 40:187–194.
- van den Heuvel MP, Hulshoff Pol HE. 2010. Exploring the brain network: a review on resting-state fMRI functional connectivity. *Eur Neuropsychopharmacol* 20:519–534.
- Vanhatalo S, Palva JM, Holmes MD, Miller JW, Voipio J, Kaila K. 2004. Infralow oscillations modulate excitability and interictal epileptic activity in the human cortex during sleep. *Proc Natl Acad Sci U S A* 101:5053–5057.
- Vanhatalo S, Tallgren P, Andersson S, Sainio K, Voipio J, Kaila K. 2002. DC-EEG discloses prominent, very slow activity patterns during sleep in preterm infants. *Clin Neurophysiol* 113:1822–1825.
- Vanhatalo S, Tallgren P, Becker C, Holmes MD, Miller JW, Kaila K, Voipio J. 2003. Scalp-recorded slow EEG responses generated in response to hemodynamic changes in the human brain. *Clin Neurophysiol* 114: 1744–1754.
- Vanhatalo S, Voipio J, Kaila K. 2005. Full-band EEG (FbEEG): an emerging standard in electroencephalography. *Clin Neurophysiol* 116:1–8.
- Veer IM, Beckmann CF, van Tol M-J, Ferrarini L, Milles J, Veltman DJ, et al. 2010. Whole brain resting-state analysis reveals decreased functional connectivity in major depression. *Front Syst Neurosci* 4:1–10.
- Voipio J, Tallgren P, Heinonen E, Vanhatalo S, Kaila K. 2003. Millivolt-scale DC shifts in the human scalp EEG: evidence for a nonneuronal generator. *J Neurophysiol* 89: 2208–2214.
- Worsley K, Friston K. 1995. Analysis of fMRI time-series revisited—again. *Neuroimage*. 2:173–181.

Address correspondence to:

Sheila D. Keilholz  
 Department of Biomedical Engineering  
 Emory University  
 1760 Haygood Dr., HSRB W230  
 Atlanta, GA 30322

E-mail: sheila.keilholz@bme.gatech.edu